Electronic Supplementary Material (ESI) for Physical Chemistry Chemical Physics.

Electronic Supplementary Information for "Understanding photochemical pathways of laser-induced metal ion reduction through byproduct analysis"

Laysa M. Frias Batista, Michael Moody, Chamari Weththasingha, Ella Kaplan, Irtiza Faruque, M. Samy El-Shall, and Katharine Moore Tibbetts

∗ kmtibbetts@vcu.edu

SI Spectroscopic assay methods and calibration

The most widely accepted methods for measuring free chlorine (Cl_2, ClOH, ClO^-) are based on use of N,N-diethyl-p-phenylenediamine (dpd^{2+}).[1–3] This molecule is used as an indicator because its initial oxidation product is a semiquinoid free radical ($dpd^{2+\cdot}$) that is highly coloured and relatively stable. The oxidation of dpd^{2+} is shown in the scheme below:

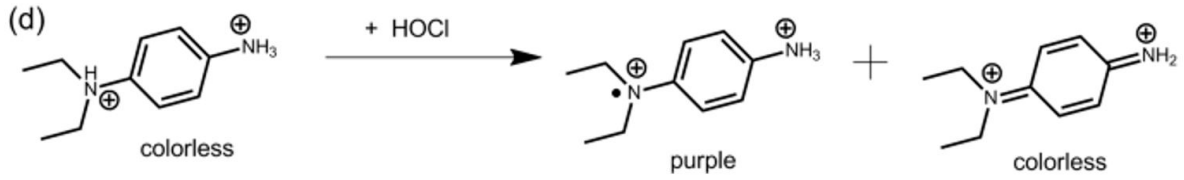

DPD oxidation reactions

The $dpd^{2+\cdot}$ absorption spectrum exhibits a doublet peak with maxima at 511 and 551 nm.[2,4] The intensity of the magenta color is related to the amount of oxidizing agent present in solution. Even though the semiquinoid free radical has resonance stabilization, it is it susceptible to further oxidation to a less stable colorless quinoid product. In order to

minimize further oxidization of the semiquinoid, it is necessary that DPD reagent remains in excess relative to oxidant concentration.

A calibration curve was constructed by measuring the absorbance at 551 nm of DPD reagent (4.3 mM) after it reacted with permanganate ($KMnO_4$) solutions with ranging concentrations of 0.42 μM to 44 μM (Figure S1). These $KMnO_4$ standards cover the chlorine equivalent range of 2.1 μM to 220 μM. The $KMnO_4$ solution used to produce the calibration curve was standardized by titrating weighed amounts of sodium oxalate, following the procedure in ref 5. Because DPD reagent solutions are subject to oxidation from atmospheric and dissolved oxygen, stock solutions of DPD (100 mM) were prepared fresh before each experiment.

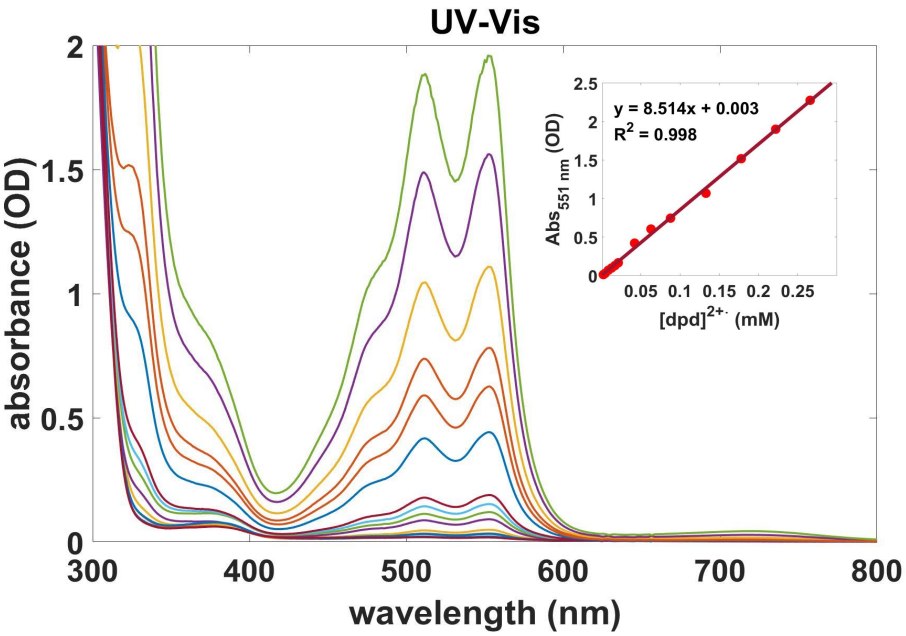

Figure S1: Absorption spectra of the $dpd^{2+\cdot}$ generated by addition of $KMnO_4$ with concentrations ranging from 0.42 μM to 44 μM.

The titanium sulfate assay for H_2O_2 has been described in detail elsewhere.[6,7] A calibration curve was constructed by measuring the absorbance of pertitanic acid after reacting 25 mM $Ti(SO_4)_2$ with aqueous solutions of 0.5 – 2.5 mM H_2O_2 (Figure S2).

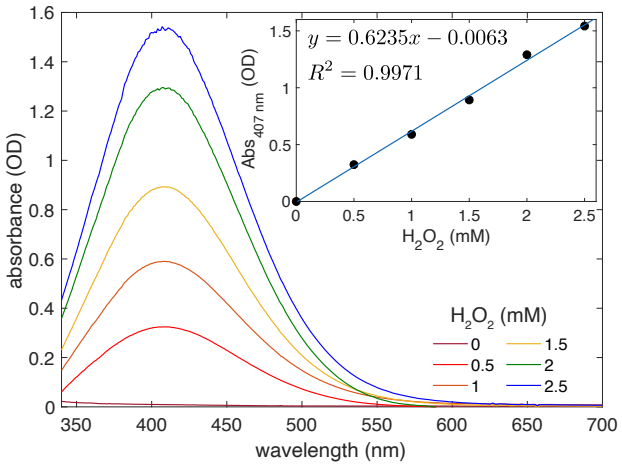

Figure S2: Absorption spectra of pertitanic acid generated by addition of varying concentrations of H_2O_2 solution.

SII Supplemental Figures for Section 3.1

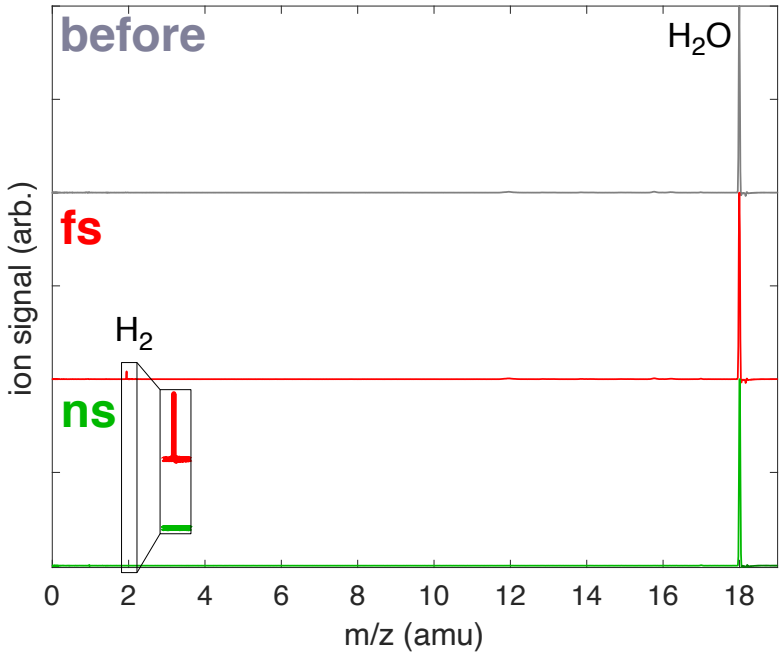

Figure S3: Mass spectra of water before laser processing (grey); after 10 minutes fs laser processing (red); after 60 minutes ns laser processing (green). Water at m/z 18 is the only peak present prior to laser processing. Fs laser processing produces H_2 as seen by the new peak at m/z 2. No H_2 is observed from ns laser processing.

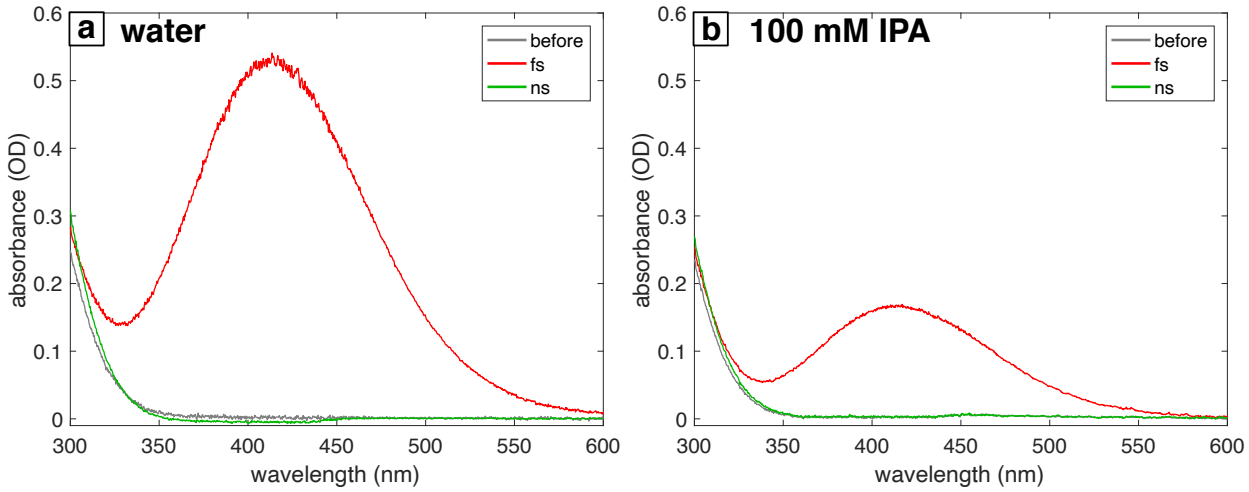

Figure S4: Absorbance spectra of laser-processed water (a) and 100 mM IPA (b) after addition of $Ti(SO_4)_2$. Solutions were processed with the fs laser for 3 minutes or with the ns laser for 30 minutes. Spectra of solutions before laser processing are shown in grey; after fs laser processing in red; after ns laser processing in green. The pertitanic acid peak at 407 nm indicates the presence of H_2O_2. The lower absorbance for 100 mM IPA is expected due to its scavenging activity towards $OH\cdot$ radicals.[8] No H_2O_2 is formed during ns laser processing.

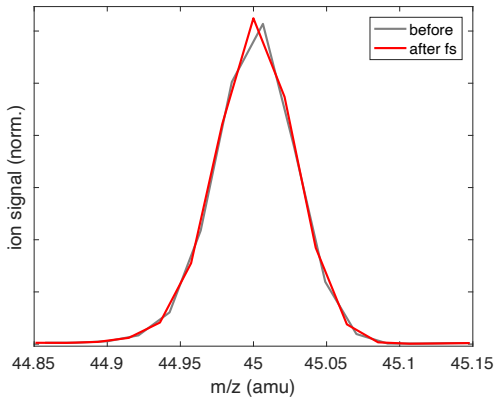

Figure S5: Magnification of m/z 45 peak from mass spectra of aqueous IPA before (grey) and after (red) femtosecond laser processing. The slight shift in peak shape results in the small negative and positive features in the difference spectra seen in Figure 1b.

SIII Supplemental Figures for Section 3.2

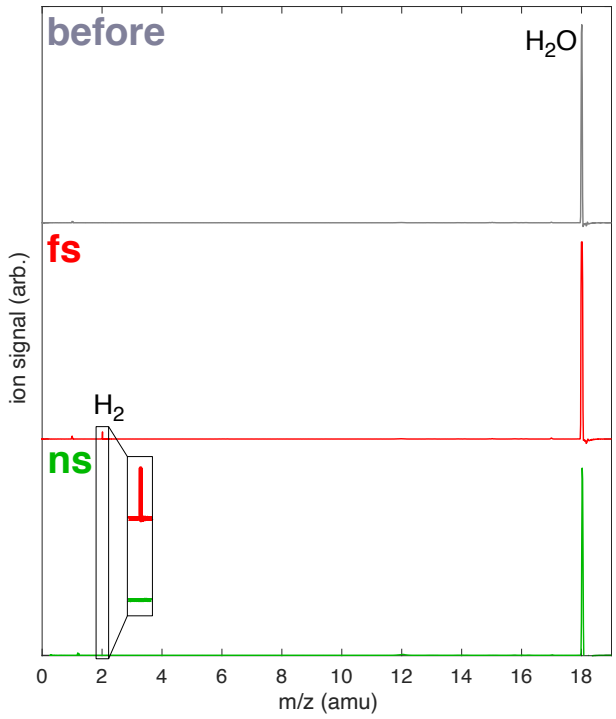

Figure S6: Raw spectra before (grey) and after femtosecond (red) or nanosecond (green) laser processing of Ag^+ in water. The inset shows production of H_2 at m/z 2 with femtosecond laser processing only.

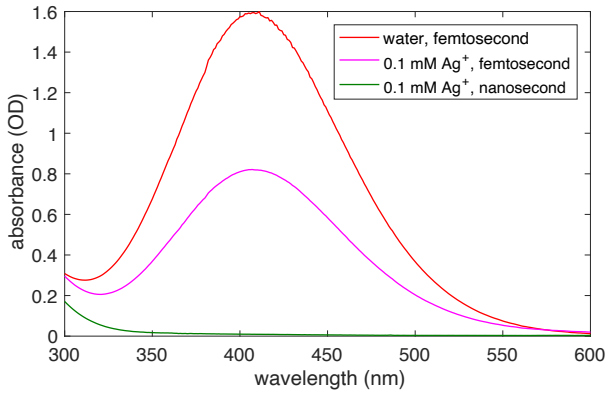

Figure S7: Absorbance spectra after addition of titanium sulfate: water (red) and 0.1 mM Ag^+ (magenta) processed with the femtosecond laser for 10 minutes; 0.1 mM Ag^+ processed with the nanosecond laser for 40 minutes (green).

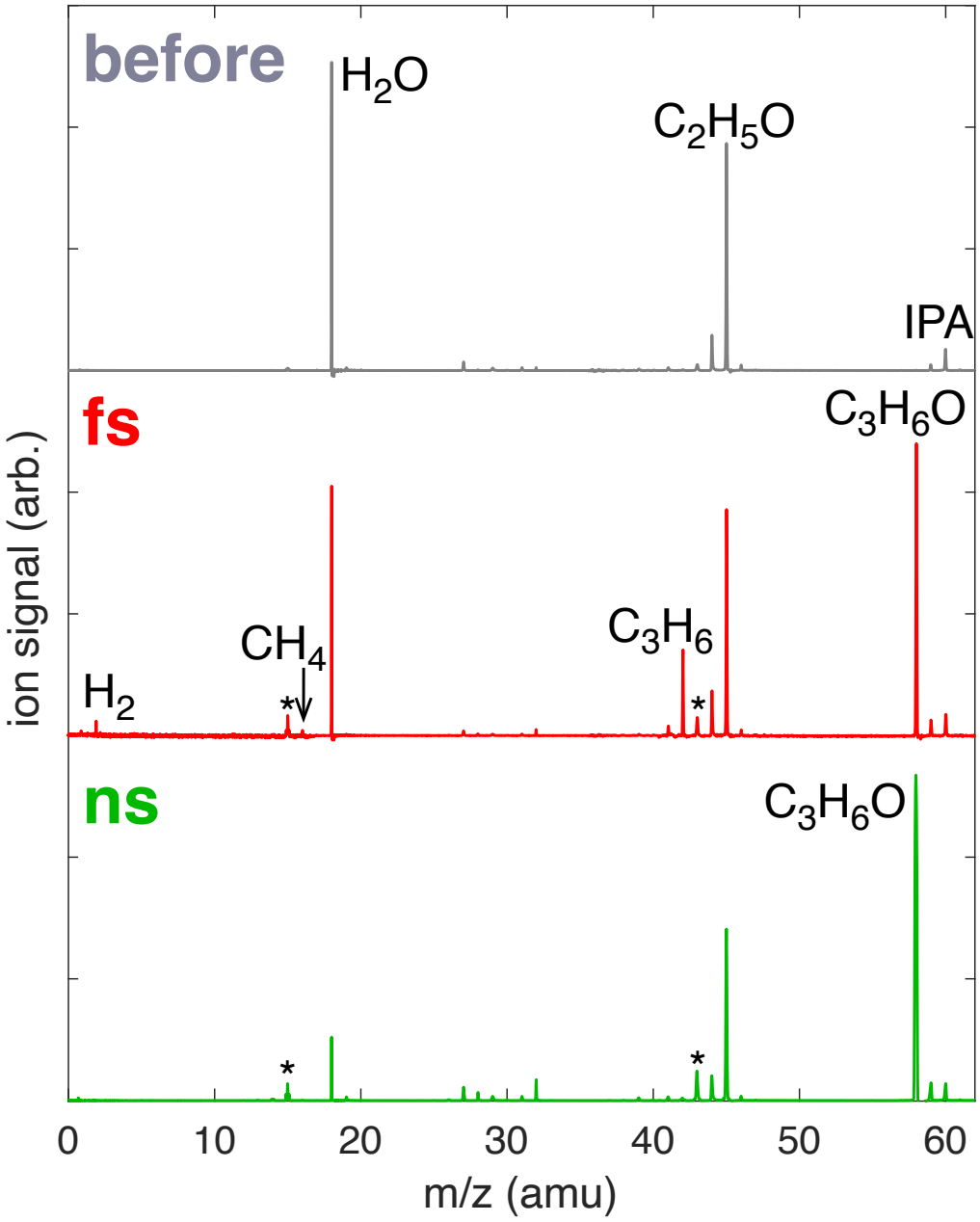

Figure S8: Raw mass spectra before (grey) and after femtosecond (red) or nanosecond (green) laser processing of 1 mM Ag^+ in 100 mM IPA. Femtosecond laser processing produces the same products seen in Figure 1 of the main work: H_2, CH_4, propene, and acetone. Nanosecond laser processing produces acetone exclusively as a new product. Peaks marked with a $*$ denote fragmentation products of acetone.

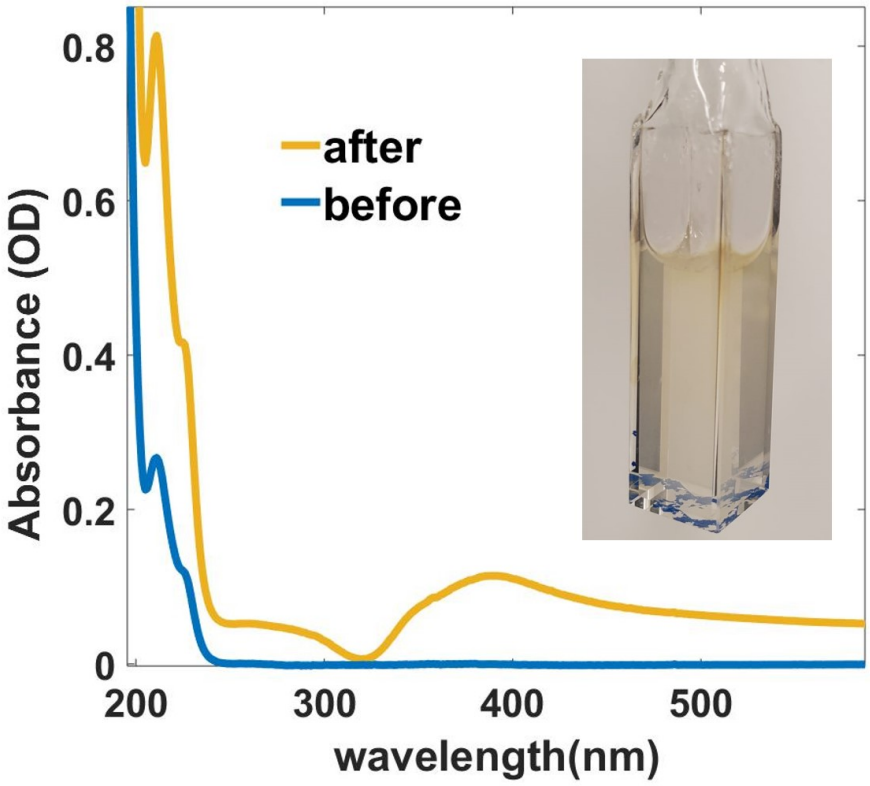

Figure S9: Absorbance spectra of an aqueous solution of 1 mM $AgClO_4$ and 100 mM IPA before and after nanosecond laser processing showing SPR feature of AgNPs centered at $\lambda \sim 400$ nm. Inset shows a photograph of the solution after laser processing.

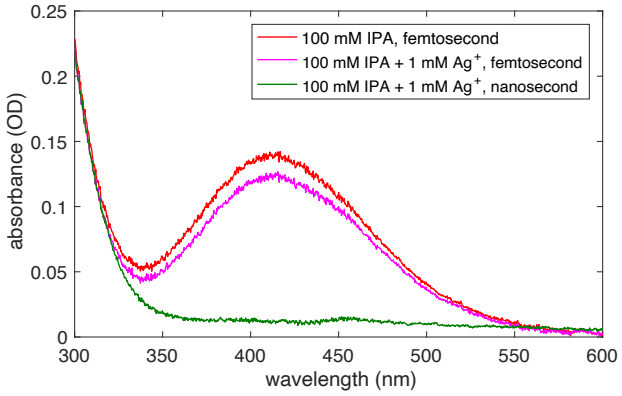

Figure S10: Absorbance spectra after addition of titanium sulfate: 100 mM IPA (red) and 1 mM Ag^+ in 100 mM IPA (magenta) processed with the femtosecond laser for 3 minutes; 1 mM Ag^+ in 100 mM IPA processed with the nanosecond laser for 30 minutes (green).

SIV Supplemental Data for Section 3.3

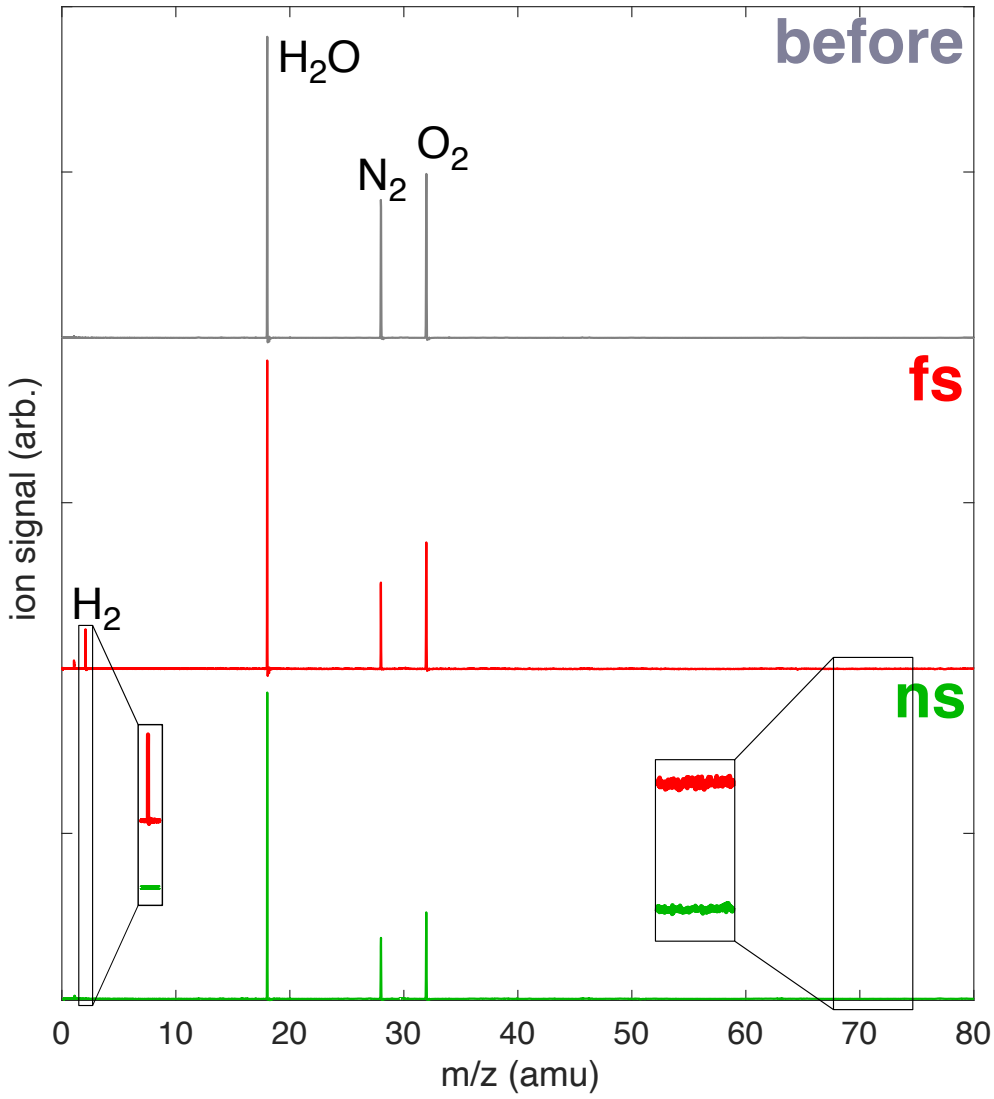

Figure S11: Raw mass spectra before (grey) and after femtosecond (red) or nanosecond (green) laser processing of 1 mM $[AuCl_4]^-$ in water. H_2 is produced during femtosecond laser processing, but not during nanosecond laser processing. The magnified noise in the range m/z 69–75 shows that no Cl_2 is formed under either condition.

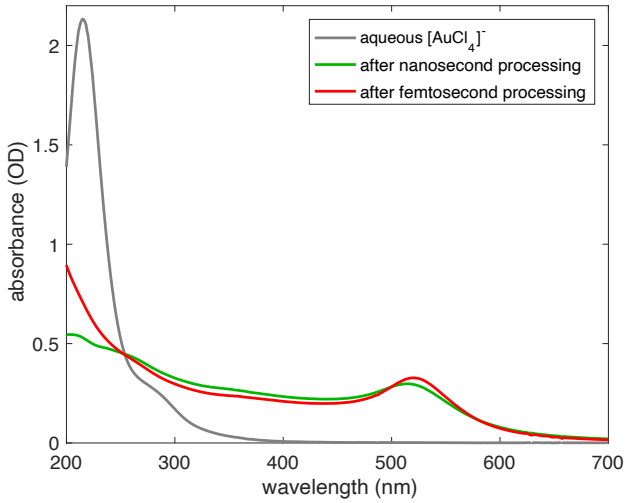

Figure S12: Absorbance spectra of 0.1 mM aqueous $[AuCl_4]^-$ (grey) and $[AuCl_4]^-$ solutions after femtosecond (red) and nanosecond (green) laser processing. The disappearance of the Ligand-metal charge transfer peak from $[AuCl_4]^-$ at 215 nm and emergence of LSPR peak around 520–530 nm indicate complete conversion to Au NPs. The higher absorbance from 200–250 nm in the femtosecond sample is due to H_2O_2.

solution	laser	[pertitanic acid] (mM)	$[dpd^{\cdot 2+}]$ (mM)
water	fs	2.52 ± 0.12	0.103 ± 0.010
0.1 mM $[AuCl_4]^-$	fs	2.29 ± 0.07	0.133 ± 0.018
water	ns	0.004 ± 0.007	0.0001 ± 0.0001
0.1 mM $[AuCl_4]^-$	ns	0.009 ± 0.010	0.0038 ± 0.0001

Table S1: Quantified yields of pertitanic acid and $dpd^{\cdot 2+}$ in samples of water and 0.1 mM $[AuCl_4]^-$ subject to femtosecond and nanosecond laser irradiation. Error bars denote standard deviation from at least 5 replicates for each condition.

References

[1] G. Gordon, D. Sweetin, K. Smith and G. Pacey, *Talanta (Oxford)*, 1991, **38**, 145–149.

[2] D. Harp and C. C. Hach, *Current Technology of Chlorine Analysis for Water and Wastewater*, Hach Company, Loveland, CO, USA, 2003.

[3] H. E. Moore, M. J. Garmendla and W. J. Cooper, *Environmental Science and Technology*,

1984, **18**, 348–353.

[4] J. Zou, H. Cai, D. Wang, J. Xiao, Z. Zhou and B. Yuan, *Chemosphere (Oxford)*, 2019, **224**, 646–652.

[5] R. S. McBride, *J. Am. Chem. Soc.*, 1912, **34**, 393–416.

[6] G. Eisenberg, *Ind. Eng. Chem. Anal. Ed.*, 1943, **15**, 327–328.

[7] V. K. Meader, M. G. John, C. J. Rodrigues and K. M. Tibbetts, *J. Phys. Chem. A*, 2017, **121**, 6742–6754.

[8] L. M. Frias Batista, V. K. Meader, K. Romero, K. Kunzler, F. Kabir, A. Bullock and K. M. Tibbetts, *J. Phys. Chem. B*, 2019, **123**, 7204–7213.